A cooperative control for the reserve management of isolated microgrids

A cooperative control for the reserve management of isolated microgrids

A. Cagnano*, A. Caldarulo Bugliari, E. De Tuglie

Dipartimento di Ingegneria Elettrica e dell'Informazione – DEI, Politecnico di Bari, Via Re David, 200, 70125 Bari, Italy

HIGHLIGHTS

- A cooperative control for reserve management of isolated microgrids is developed.
- The methodology is based on the sensitivity theory involving the Lyapunov theorem.
- It is aimed at maximizing the overall spinning reserve of an isolated microgrid.
- It is used in the real-time to alleviate the regulation burden of the master unit.
- Test results demonstrated the controller's ability to be self-adaptive.

ABSTRACT

The purpose of this paper is to examine how a coordinated control strategy for managing the active power reserve in isolated microgrids is presented. This methodology can be applied in those microgrids where a specified generator assumes the role of the isochronous generator for the overall system. The derived algorithm evaluates control actions in the on-line environment by solving a constrained dynamic optimization problem aimed at maximizing the overall spinning reserve and, in particular, the reserve offered by the master unit equipped with the isochronous governor controller. The solution of this problem is obtained by adopting the direct Lyapunov theorem applied to the Sensitivity theory, ensuring the algorithm's stability.

Tests performed on the experimental microgrid, which has been built at the Polytechnic University of Bari, demonstrated the ability of the proposed methodology to share the regulation burden among all sources and storage systems, establishing adequate reserve margins of the master unit.

1. Introduction

Microgrids are becoming more and more interesting due to their ability to alleviate consequences of sudden grid outages, ensuring a reliable and uninterrupted energy supply by producing the required energy for the overall system and related ancillary services. However, due to the absence of the main grid support, the occurrence of power disturbances may move these systems to an insecure operating point of the stability region. This is much more likely to occur in microgrids having low or even null inertia. The need of real-time control strategies able to maintain the power balance at all times, has aroused the interest of many researchers in developing several control solutions [1–8], a minimum cost control strategy able to share the total load demand among all energy sources has been developed by tuning the Distributed Generators (DG) droop gradients, obtaining an optimal dispatch including non-programmable renewable energy sources. With the same aim, papers [9–13] suggest an optimization problem based on the mixed integer linear programming (MILP) method, whereas in [14] a multi-period gravitational search algorithm (MGSA) is developed. Nonetheless, it is worth noting that most commercially available inverters are not equipped with the droop control, therefore the adoption of droop control strategies will require the development of *ad-hoc* devices as is the case of the microgrids developed in [15–19]. At this stage in the development of microgrids, the vast majority of them are based on the master/slave controller [20–25]. In these microgrids the real-time power balancing is much more complex than droop-controlled ones. In fact, as outlined in [25], in these microgrids the generating unit acting as the master generator may not have sufficient generation capacity to cover all possible unbalances that could occur within the island. Therefore, a cooperative control strategy able to alleviate the regulation burden of the master generator is needed. To comply with this exigency, several control strategies have been developed in the last years. In [26–28] the centralized control strategies are able to share the total load demand among all microsources and storage devices which are suggested. By these approaches, control actions are evaluated by adopting an economic dispatch algorithm, considering all programmable as well as non-programmable sources, storage devices and loads with their uncertainties

* Corresponding author.
E-mail address: alessia.cagnano@poliba.it (A. Cagnano).

and disturbances. Power reserve margins are treated as constraints of the optimization problem by taking into account the day-ahead electricity market and reserve costs [29–31]. Focusing on the optimization of the spinning reserve of isolated microgrids, centralized controllers developed in [32–41] share the control burden among all microsources by adopting the Particle Swarm Optimization (PSO) algorithm based on the Monte Carlo method [32], the Mixed-Integer Linear Programming (MILP) [33], and the Conservative Power Theory [34–41].

Following the same aim, in this paper a real-time coordinated control strategy able to ensure an adequate security level in an isolated microgrid is proposed. Control actions are evaluated by solving a constrained dynamic optimization problem aimed at maximizing the overall spinning reserve and, in particular, the reserve offered by the master unit acting as the isochronous regulator. The solution of this optimization problem is evaluated by adopting the direct Lyapunov theorem applied to the Sensitivity theory, ensuring the algorithm's stability. The developed control strategy has been tested on the Experimental Microgrid built at the Polytechnic University of Bari.

2. Reserve classification for master-slave based microgrids

When operated in the isolated mode, master-slave controlled microgrids need a generator or a storage device which will control the voltage and the frequency, thus recovering any disturbance occurring on the system according to its capability curve. The required regulating power needs to be instantaneously provided by the master unit, otherwise the system would collapse. For microgrids having minimal or even null inertia, this phenomenon can be reached in tens of milliseconds. Hence, corrective control actions need to be promptly evaluated and applied in order to avoid the system blackout. This exigency cannot be supplied with slave devices with their slow reserves. Moreover, a practical communication system has latencies which are too large for primary control. In a sense, for master-slave controlled microgrids, the classification of the available reserve needs to be revised accordingly. The spinning reserve can be divided into the "primary reserve", which is then able to be developed in tens of milliseconds by the master unit, and the "secondary reserve", with an action ranging from seconds up to tens of seconds. Since the primary reserve is managed by the isochronous regulator of the master unit, a reasonably small frequency error will be produced until the generator has insufficient reserve availability. Therefore, the secondary controller will move power set-points of dispatchable generators and storage devices in order to restore the fixed amount of the primary reserve of the master controller.

The "stand-by" reserve will be constituted by all generating units and storage devices which can be available in tens of seconds up to a few minutes. Finally, the tertiary control level is aimed at performing the optimal dispatch of energy sources as proposed in [42]. One of the main necessities of the dispatch optimization performed at this control level, is to comply with inequality constraints related to adequate levels of reserve. For this reason, the solution of the optimization process will be power set-points of energy sources taking into account security margins for expected as well as unexpected contingencies.

3. Mathematical formulation of the cooperative control methodology

The aim of this section is to formulate a cooperative control methodology able to ensure adequate reserve margins in master-slave controlled microgrids. In this way, the derived optimization methodology will coordinate both primary and secondary reserves by controlling energy resources. For this purpose, let us consider a microgrid based on a master/slave controller consisting of $N = 1 + n_G + n_{RES} + n_S + n_L$ nodes, having one master unit, n_G dispatchable generators, n_{RES} non-dispatchable renewable sources, n_S storage devices and n_L loads. In order to formulate the overall optimization problem, the following basic elements of the procedure need to be defined.

3.1. The control variables

The variables that need to be adjusted in order to ensure a reliable and secure operation of the isolated microgrid are defined as follows:

$$\boldsymbol{u}(t) = [\boldsymbol{P}_G(t)\ \boldsymbol{P}_S(t)]^T \tag{1}$$

where

- $\boldsymbol{P}_G(t)$ is the n_G-dimensional vector of powers of all dispatchable generators involved in the reserve ancillary service.
- $\boldsymbol{P}_S(t)$ is the n_S-dimensional vector of powers at connection points of all storage devices involved in the reserve ancillary service.

Apex T denotes the transpose operator.

3.2. The objective function

The optimization problem will consist in a concurrent optimization aimed at maximizing the overall spinning reserve and it will be based on the following four error functions.

3.2.1. Primary reserve error function

During the isolated operation of the microgrid, the master generator will be called to increase or decrease its generated power output depending on unbalances occurring on the microgrid. In order to avoid possible violations of upper and lower power limits, its power output will be kept as close as possible to the specified set-point, restoring as much as possible the primary reserve of the master unit. With this aim, we define the primary reserve control error e_M^{pry} as the following scalar function:

$$e_M^{pry}(\boldsymbol{u}(t)) = P_M(t) - P_M^{set}(t) \tag{2}$$

where $P_M(t)$ is the active power produced by the selected master unit and $P_M^{set}(t)$ is its desired set-point.

Note that, in the master configuration, the isochronous regulator operates in the V-f control mode and thus it cannot comply with active power control signals coming from the secondary controller. As a consequence, the active power provided by the master unit can be regulated by managing the active powers provided by all other dispatchable sources distributed over the microgrid through the following relationship:

$$P_M(t) = \left[-\sum_{i=1}^{n_G} P_G^i(t) - \sum_{j=1}^{n_{RES}} P_{RES}^j(t) - \sum_{h=1}^{n_S} P_S^h(t) + \sum_{k=1}^{n_L} P_L^k(t) \right] \tag{3}$$

where

- $P_G^i(t)$ is the active power supplied by the generic *i-th* (for $i = 1,...,n_G$) dispatchable unit;
- $P_{RES}^j(t)$ is the active power injected by the generic *j-th* (for $j = 1,...,n_{RES}$) non-dispatchable RESs;
- $P_S^h(t)$ denotes the active power absorbed or injected by the generic *h-th* (for $h = 1,...,n_S$) storage system;
- $P_L^k(t)$ is the active power required by the generic *k-th* (for $k = 1,...,n_L$) load.

Substituting Eq. (3) into Eq. (2), the following primary reserve control error, e_M^{pry}, can be derived:

$$e_M^{pry}(\boldsymbol{u}(t)) = \left[-\sum_{i=1}^{n_G} P_G^i(t) - \sum_{j=1}^{n_{RES}} P_{RES}^j(t) - \sum_{h=1}^{n_S} P_S^h(t) + \sum_{k=1}^{n_L} P_L^k(t) \right] - P_M^{set}(t) \tag{4}$$

With this assumption, Eq. (4) is a scalar function of the vector $\boldsymbol{u}(t)$.

3.2.2. Secondary reserve error function of dispatchable generators

The aim of this cost function is to keep the reserve power offered by each dispatchable generator to be as close as possible to the set-point value, in order to preserve the optimal condition deriving from the tertiary control level.

For this purpose, the following n_G-dimensional error vector can be defined:

$$\boldsymbol{e}_G^{sec}(\boldsymbol{u}(t)) = \boldsymbol{P}_G(t) - \boldsymbol{P}_G^{set}(t) \tag{5}$$

where $\boldsymbol{P}_G^{set}(t)$ is the n_G-dimensional vector of power set points of all dispatchable generators.

3.2.3. Secondary reserve error function of storages

Contrarily, from other generators, the reserve power of storage devices can be significantly influenced by their State of Charge (SOC). Indeed, the more the SOC is close to admissible limits, the less the reserve duration is. For this reason, storage devices need to be characterized by their power reserve as well as their energy reserve. From a mathematical point of view, this condition implies that the cost function associated to storage devices needs to be split into two components. The first one is the power-related error function which can be defined as:

$$\boldsymbol{e}_{S,P}^{sec}(\boldsymbol{u}(t)) = \boldsymbol{P}_S(t) - \boldsymbol{P}_S^{set}(t) \tag{6}$$

where $\boldsymbol{P}_S^{set}(t)$ is the n_S-dimensional column vector of the specified set-point values of all storage devices involved in the reserve ancillary service. In order to maximize the reserve offered by storages, the elements of this vector are settled to zero.

The power produced or injected into a storage device can differ from the power at its connection point due to losses on interfacing devices. As a result of this, the SOC needs to be evaluated by considering the power actually absorbed or released by the storage device. Losses on interfacing devices of storage can be represented by a sum of no-load losses and current dependent losses reflecting joule effects as follows:

$$\boldsymbol{P}_S^{Loss}(t) = \boldsymbol{P}_S^0 + diag(\boldsymbol{K})\boldsymbol{P}_S(t) \circ \boldsymbol{P}_S(t) \tag{7}$$

where

- $\boldsymbol{P}_S^{Loss}(t)$ is the n_S-dimensional vector of power losses of storage devices;
- $\boldsymbol{P}_S^0$ is the n_S-dimensional vector of no-load power losses of storage devices;
- $\boldsymbol{K}$ is a n_S-dimensional column vector whose elements are positive loss coefficients denoting the power dependent losses due to Joule effects;
- $\circ$ denotes the element-by-element product operator.

Under these assumptions, the n_S-dimensional vector of power produced or injected by storage devices, $\boldsymbol{P}_B(t)$, can be expressed as:

$$\boldsymbol{P}_B(t) = \boldsymbol{P}_S(t) + \boldsymbol{P}_S^{loss}(t) \tag{8}$$

Then, the SOC of storage devices can be defined as follows:

$$\boldsymbol{SOC}_S(t) = \int_{t0}^{t} -\boldsymbol{P}_B(t)dt \tag{9}$$

where $\boldsymbol{SOC}_S(t)$ is the n_S-dimensional vector of SOCs of storage devices.

In order to maximize the duration of the reserve provided by storage devices, their state of charge should be kept as close as possible to 50% of the maximum capacity allowed. Therefore, the energy-related error function can be derived as follows:

$$\boldsymbol{e}_{S,SOC}^{sec}(\boldsymbol{u}(t)) = \left(\boldsymbol{SOC}(t) - \frac{\boldsymbol{SOC}^{max} - \boldsymbol{SOC}^{min}}{2}\right) \tag{10}$$

where $\boldsymbol{SOC}^{max}$ and $\boldsymbol{SOC}^{min}$ are n_S-dimensional vectors, which have elements that represent the maximum and minimum State Of Charge allowed for each storage device embedded into the microgrid.

3.3. The overall objective function

Based on the above assumptions, the overall $(1 + n_G + 2n_S)$-dimensional column vector of control errors can be formulated as follows:

$$\boldsymbol{e}(\boldsymbol{u}(t)) = \begin{bmatrix} e_M^{pry}(t) \\ \boldsymbol{e}_G^{sec}(t) \\ \boldsymbol{e}_{S,P}^{sec}(t) \\ \boldsymbol{e}_{S,SOC}^{sec}(t) \end{bmatrix} \tag{11}$$

With the aim to contemporaneously minimize the four types of errors, the following performance index $\mathrm{V}(\boldsymbol{u}(t))$ is defined:

$$\mathrm{V}(\boldsymbol{u}(t)) = \frac{1}{2}\boldsymbol{e}(\boldsymbol{u}(t),t)^T \boldsymbol{W}\ \boldsymbol{e}(\boldsymbol{u}(t),t) \tag{12}$$

where $\boldsymbol{W}$ is a $[(1 + n_G + 2n_s) \times (1 + n_G + 2n_s)]$-dimensional symmetric positive definite matrix, in which the coefficients weigh individual components of the performance index with respect to the objective.

The optimization of the global multi-objective function (12) requires that the following equality and inequality constraints are satisfied.

3.4. Equality constraint

3.4.1. Microgrid power balance constraint

The supply-demand balance equation can be stated as follows:

$$P_M(t) + \sum_{i=1}^{n_G} P_G^i(t) + \sum_{j=1}^{n_{RES}} P_{RES}^j(t) + \sum_{h=1}^{n_S} P_S^h(t) - \sum_{k=1}^{n_L} P_L^k(t) = 0 \tag{13}$$

3.5. Inequality constraints

3.5.1. Power-related operating constraints

The active power of generators and storages are subject to the following inequality constraints:

$$\begin{aligned} &P_{M,min} \leqslant P_M(t) \leqslant P_{M,max} \\ &P_{G,min}^i \leqslant P_G^i(t) \leqslant P_{G,max}^i \quad i = 1,\ldots,n_G \\ &P_{S,min}^h \leqslant P_S^h(t) \leqslant P_{S,max}^h \quad h = 1,\ldots,n_S \end{aligned} \tag{14}$$

where $P_{M,min}$ and $P_{M,max}$ are the minimum and the maximum power limits of the master unit; $P_{G,min}^i$ and $P_{G,max}^i$ are the minimum and the maximum power limits of the generic *i-th* dispatchable generator; $P_{S,min}^h$ and $P_{S,max}^h$ are the minimum and the maximum power limits of the generic *h-th* storage system.

3.5.2. Energy-related operating constraints

In order to guarantee the operability of storage systems as reserve power providers, their SOCs must be constrained to acceptable ranges:

$$SOC_{S,min}^h \leqslant SOC_S^h(t) \leqslant SOC_{S,max}^h \quad h = 1,\ldots,n_S \tag{15}$$

where $SOC_{S,min}^h$ and $SOC_{S,max}^h$ are the minimum and the maximum SOC limits of the generic *h-th* storage system.

3.6. The overall optimization problem

Looking at the above assumptions, the overall optimization problem can be stated as follows:

$$min_{\boldsymbol{u}}\ \mathrm{V}(\boldsymbol{u}(t)) = min_{\boldsymbol{u}}\left(\frac{1}{2}\boldsymbol{e}(\boldsymbol{u}(t))^T\boldsymbol{W}\boldsymbol{e}(\boldsymbol{u}(t))\right) \tag{16}$$

subject to:

$$P_M(t) + \sum_{i=1}^{n_G} P_G^i(t) + \sum_{j=1}^{n_{RES}} P_{RES}^j(t) + \sum_{h=1}^{n_S} P_S^h(t) + \sum_{k=1}^{n_L} P_L^k(t) = 0 \tag{17}$$

$$\begin{aligned} &P_{M,min} \leqslant P_M(t) \leqslant P_{M,max} \\ &P_{G,min}^i \leqslant P_G^i(t) \leqslant P_{G,max}^i \quad i = 1,\ldots,n_G \\ &P_{S,min}^h \leqslant P_S^h(t) \leqslant P_{S,max}^h \quad h = 1,\ldots,n_S \end{aligned} \tag{18}$$

$$SOC_{S,min}^h \leqslant SOC_S^h(t) \leqslant SOC_{S,max}^h \quad h = 1,\ldots,n_S \tag{19}$$

4. The on-line algorithm

An approach for solving the problem stated in (16)–(19) consists in developing a fictitious dynamic system, with state variables which are represented by the defined control variables. The solution of the optimization problem can be obtained by finding the equilibrium point (if any) of this dynamic system.

To set up the dynamic model, we assume the performance index defined in Eq. (12) to be a time dependent Lyapunov function. In actual fact, noting is a quadratic form, this is an always semi-positive definite function. Its time derivative will be:

$$\dot{\mathrm{V}}(\boldsymbol{u}(t)) = \boldsymbol{e}(\boldsymbol{u}(t))^T\boldsymbol{W}\,\dot{\boldsymbol{e}}(\boldsymbol{u}(t)) = \boldsymbol{e}(\boldsymbol{u}(t))^T\boldsymbol{W}\left(\frac{\partial \boldsymbol{e}(\boldsymbol{u}(t))}{\partial \boldsymbol{u}(t)}\right)\dot{\boldsymbol{u}}(t) \tag{20}$$

According to the Lyapunov theory, if the time derivative of $\mathrm{V}(\boldsymbol{u}(t))$, $\dot{\mathrm{V}}(\boldsymbol{u}(t))$can be made negative semidefinite, the existence of an equilibrium point is guaranteed. Therefore, in order to force $\dot{\mathrm{V}}(\boldsymbol{u}(t))$to be an always-negative semidefinite function, the following artificial dynamic system is considered:

$$\dot{\boldsymbol{u}}(t) = -k\left(\frac{\partial \mathrm{V}(\boldsymbol{u}(t))}{\partial \boldsymbol{u}(t)}\right)^T = -k\left(\frac{\partial \boldsymbol{e}(\boldsymbol{u}(t))}{\partial \boldsymbol{u}(t)}\right)^T\boldsymbol{W}^T\boldsymbol{e}(\boldsymbol{u}(t)) \tag{21}$$

where $k \in \Re^+$.

Substituting (21) into (20), a quadratic form of the desired negative semidefinite function $\dot{\mathrm{V}}(\boldsymbol{u}(t),t)$ can be obtained:

$$\dot{\mathrm{V}}(\boldsymbol{u}(t)) = -k\boldsymbol{e}(\boldsymbol{u}(t))^T\boldsymbol{W}\left(\frac{\partial \boldsymbol{e}(\boldsymbol{u}(t))}{\partial \boldsymbol{u}(t)}\right)\left(\frac{\partial \boldsymbol{e}(\boldsymbol{u}(t))}{\partial \boldsymbol{u}(t)}\right)^T\boldsymbol{W}^T\boldsymbol{e}(\boldsymbol{u}(t)) \tag{22}$$

The adoption of the Lyapunov method ensures the existence of an equilibrium point for the dynamic system (21) and this will coincide with the minimum of the given Lyapunov function (12). Consequently, integrating Eq. (21) in the time domain, the control laws $\boldsymbol{u}(t)$ can be obtained:

$$\boldsymbol{u}(t) = -k\int\left(\frac{\partial \boldsymbol{e}(\boldsymbol{u}(t))}{\partial \boldsymbol{u}(t)}\right)^T\boldsymbol{W}^T\boldsymbol{e}(\boldsymbol{u}(t))\,dt \tag{23}$$

Note that, with the above assumptions, Eq. (23) gives rise to a stable solution of the optimization problem. Following a contingency occurrence in the system, the autonomous dynamic system (21) produces control laws moving the operating point in another equilibrium point where the Lyapunov function $\mathrm{V}(\boldsymbol{u}(t))$ is minimal.

The developed procedure can be implemented on the basis of the flow chart shown in Fig. 1.

5. Test system and simulation results

The performance of the proposed approach was tested on the experimental microgrid built at the Polytechnic University of Bari, Italy, where a one-line diagram of this is reported in Fig. 2.

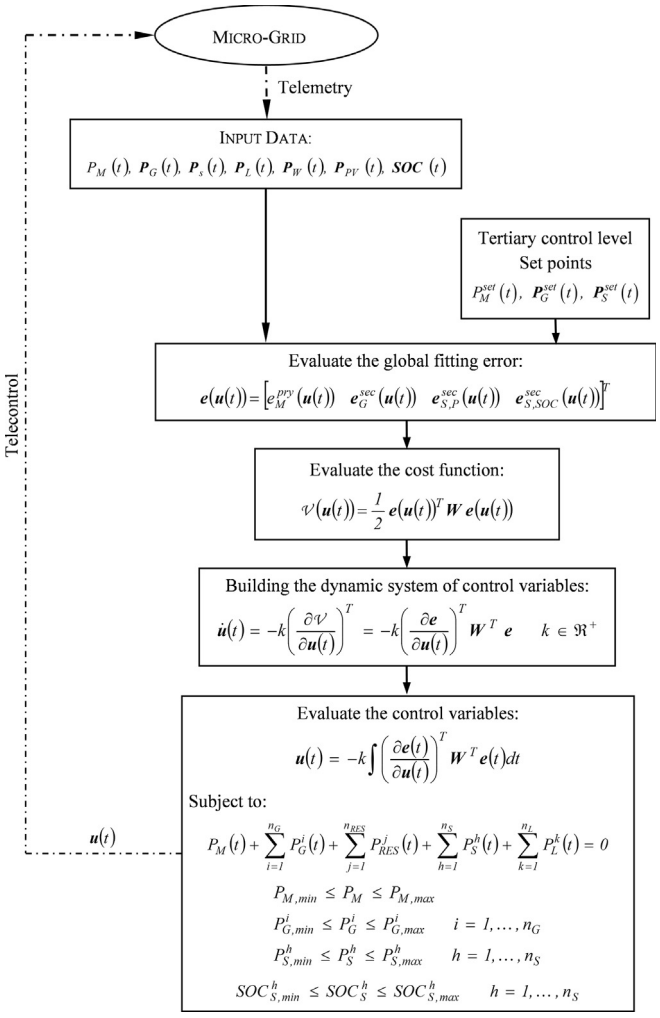

Fig. 1. Flow-chart of the proposed algorithm.

The 400 V microgrid is connected to the 9 kV distribution network through a 1250 kVA transformer. The microgrid includes a 120 kWe gas-fueled CHP system, a 30 kWe natural gas fueled micro-turbine, a 50 kW photovoltaic power generation system, a 60 kW wind turbine generator emulator, a 60 kW–180 kWh Battery Energy Storage System (BESS) along with a 200 kW by-pass inverter and 2 × 150 kVA inverter-based programmable loads. Each component is interfaced to the microgrid through an inverter, thus obtaining an inertialess system. Details on the system can be found in [24,25]. With the exception of the photovoltaic system, all the microgrid devices can be programmed in order to follow a specified power trajectory in the time domain. Even if power deriving from the photovoltaic plant needs to be simulated, as in this case, the by-pass inverter can be used. With this powerful facility several control methodologies can be compared under the same test conditions.

The master generator can be chosen among the CHP, the BESS and the microturbine. Nevertheless, none of these generators/storage have enough regulation capacity to fulfil any unbalance occurring on the system.

In order to verify the effectiveness of the proposed methodology, a comparative analysis with an optimal dispatching policy was performed in the three following cases:

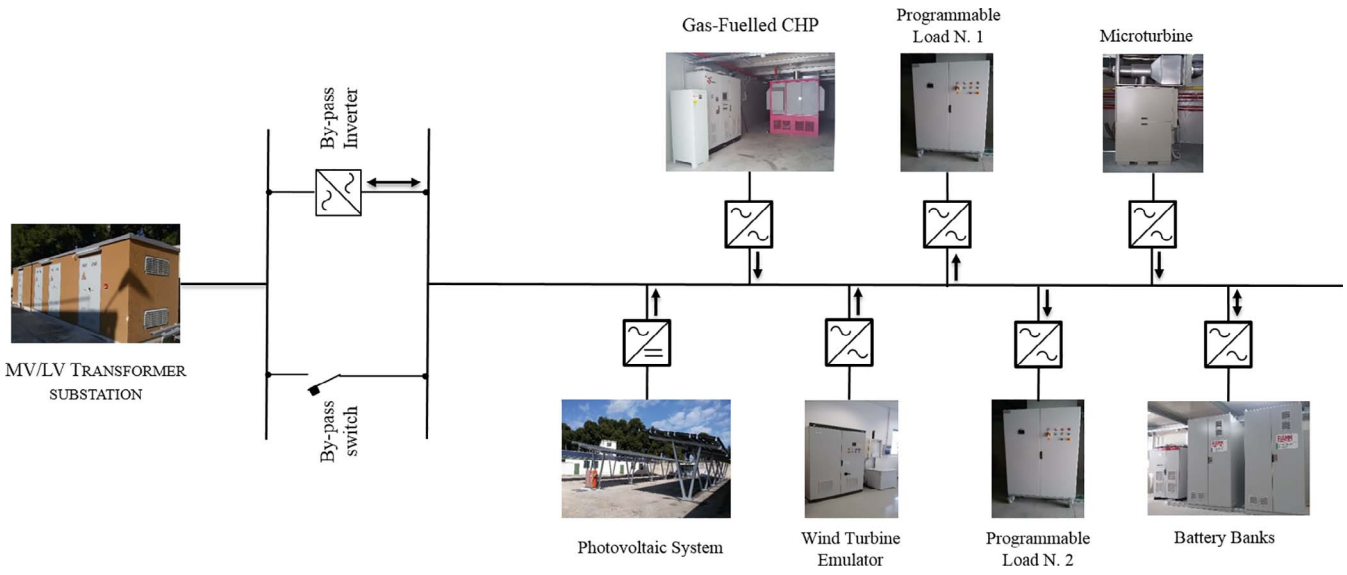

Fig. 2. The one-line diagram of the experimental microgrid.

- ***Case 1 – One day analysis.*** In order to test the proposed controller under stressed conditions, the working day of October, 6th 2016 was chosen. This day was characterized by frequent and large power fluctuations of PV and wind generation.
- ***Case 2 – Microturbine failure.*** This experimental test was performed in order to check the controller's ability to recover a contingency occurring on the system and to restore adequate margins of the primary reserve.
- ***Case 3 – Annual analysis.*** This simulation test was aimed at checking the controller's performance on a longer time frame than on the single day.

For all the tests, the microgrid was operated in isolation with the CHP system acting as the master generator. Moreover, the specified set-point deriving from the tertiary control level for the master unit was assumed equal to 50% of its rated power ($P_{CHP}^{set} = 60$ kW).

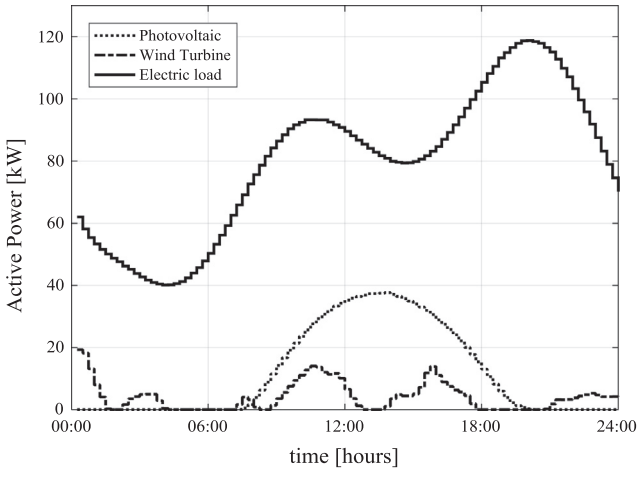

Fig. 3. The day-ahead forecast of the load demand, wind and photovoltaic.

5.1. Case 1 – One day analysis

This test aimed at investigating algorithm's performance on the working day of October, 6th 2016 in Bari. For these purposes, we compared results obtained from the developed algorithm with those deriving from the system operated by means of an economic dispatch. In doing this, a day-ahead operation planning of the microgrid was preliminarily performed. As in common practice, reserve margins were taken into account by limiting the power output of generating units equipped with primary controllers as a percentage of the forecasted uninterrupted load. Thus, in the case of this test, the reserve margins for each planning period (15 min) were set to 15% of the forecasted uninterrupted load for the same period. The uninterrupted load was assumed to be equal to 100% of the total load supplied by the experimental microgrid. The economic dispatch determined the quarter-hour production plan of the CHP generator, the microturbine and the BESS on the basis of the day-ahead forecast of the load demand, the forecasted wind and photovoltaic power outputs. Recorded data of a typical residential area characterized by about 330 houses, were used to simulate the day-ahead load forecast by sampling the data for each quarter-hour and by adding white noise representing a load forecast error equal to 10% of the critical load. The same procedure on data recorded at a real wind farm located in the Southern Italy was adopted in order to obtain the day-ahead wind power production forecast. In this case we assumed a forecasting error equal to ± 30% for each quarter-hour. The day-ahead PV forecasted power was obtained by means of available meteorological data at the microgrid site. Fig. 3 shows the day-ahead forecast, sampled at each quarter-hour, of the load demand, the wind power and the photovoltaic power.

Starting from this data, the day-ahead economic dispatch was performed. Particularly, we assumed nonprogrammable renewable sources to be operated under the priority dispatch policy. The following quadratic fuel cost functions for the CHP and the microturbine were assumed:

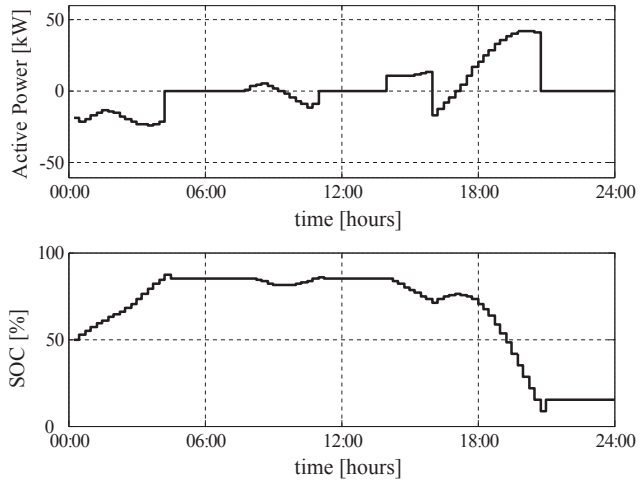

Fig. 4. Planned operation of the BESS.

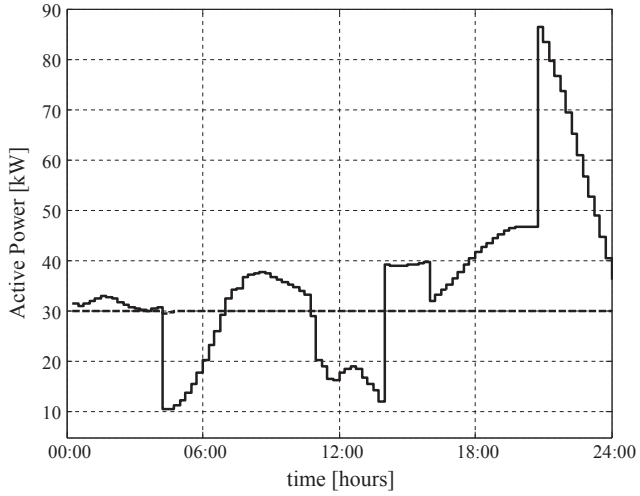

Fig. 5. Quarter-hour production plan of the CHP engine (solid line) and the Microturbine (dotted line).

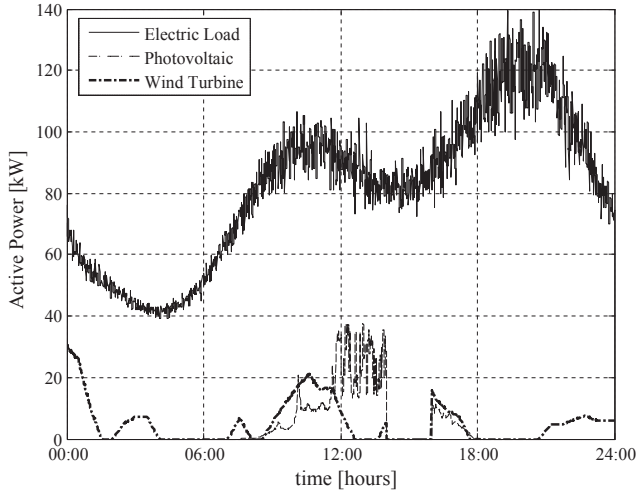

Fig. 6. Daily profiles of load, PV and wind generation.

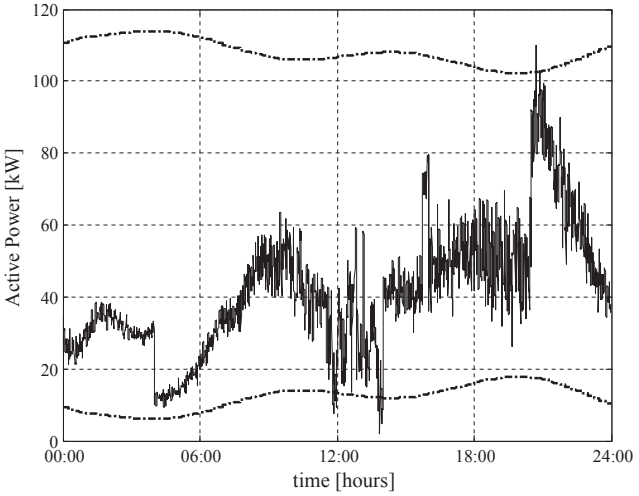

Fig. 7. Daily profile of the CHP system: produced power (solid line) and reserve margins (dashed-dotted line).

$$C_{CHP}(P_{CHP}) = 0.000178\,P_{CHP}^2 + 0.233564\,P_{CHP} + 2.288581 \quad [€/h]$$
$$C_{MT}(P_{MT}) = 0.0005\,P_{MT}^2 + 0.2135\,P_{MT} + 1.4406 \quad [€/h] \tag{24}$$

The day-ahead charge/discharge schedule of the BESS was determined based on the energy price at each quarter-hour. In particular, the BESS was charged/discharged during the lower/higher price hours. Limits on the maximum and the minimum charge/discharge power as well as on the SOC were included. The resulting schedule of the BESS is shown in Fig. 4.

The obtained quarter-hour day-ahead operation plan for the CHP and the microturbine is shown in Fig. 5.

As can be noted, due to the lower operating costs, the microturbine was scheduled to its maximum active power (30 kW) for the whole day.

In order to always preserve the established reserve margins, a preventive control based on the load/generation shedding technique was implemented. Every 15 min, the preventive controller verified that the system operating point planned for the next period was compatible with the adopted reserve margins in order to cover any possible forecasting error and variability of the load and the photovoltaic as well as wind productions. If the production plan threatened the scheduled reserve, the preventive controller evaluated the minimum amount of the load or generation to be shed. In this paper, following suggestions in [26,43–46], the reserve margins were set to 15% of the forecasted uninterrupted load.

The real time operation was tested on the experimental microgrid by adopting recorded data having a sampling time equal to 1 min. Fig. 6 shows the load profile as well as the PV and wind power productions. As can be noted, due to the excessive power production of renewable energy sources, a generation shedding was implemented for two hours of the day.

Fig. 7 shows the actual operation of the CHP. As can be noted, the actual operation of the CHP significantly deviated from the scheduled one (Fig. 5). In particular, during midday hours and at 21:00, the reserve limits were violated. In these operating points, the CHP was operated close to the setting values of its protective relays.

The proposed methodology was experimentally tested under the same conditions giving rise to the generation daily profile shown in Fig. 8.

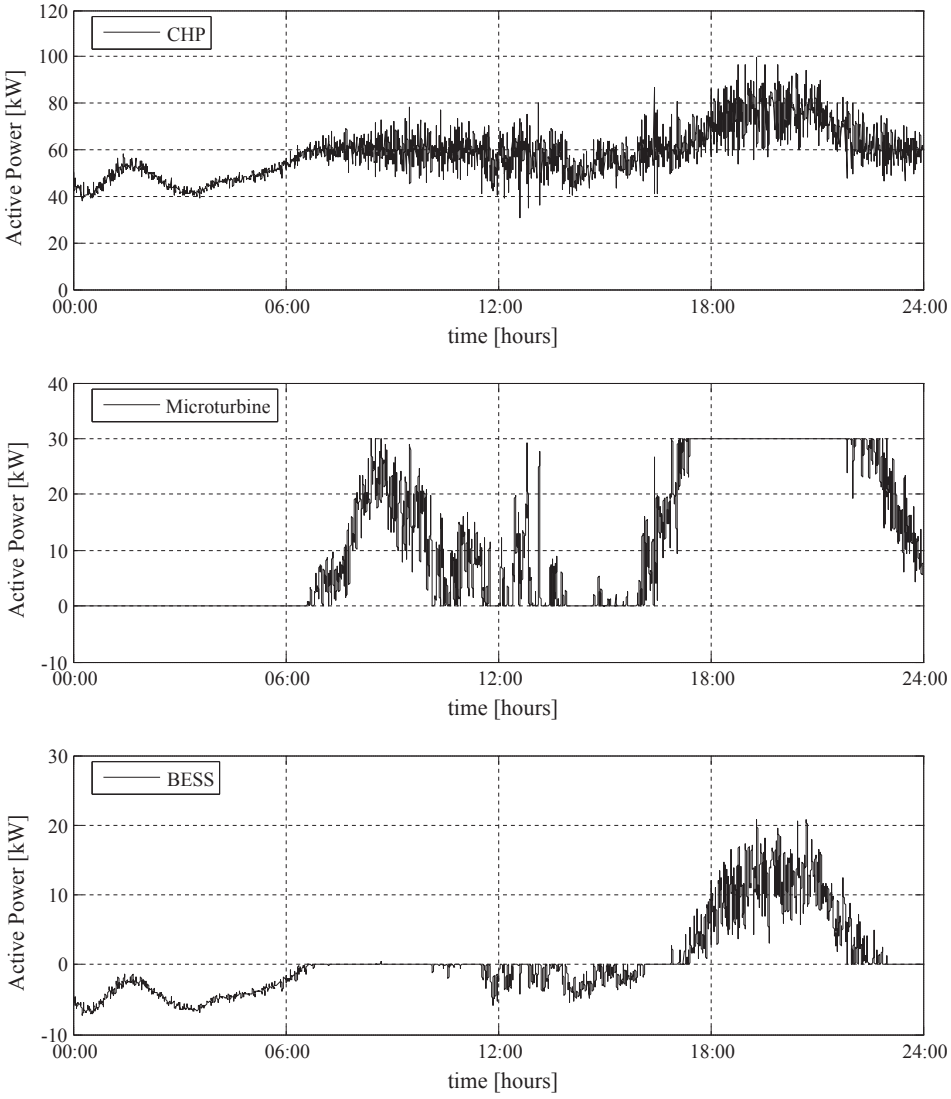

Fig. 8. Time domain behavior of the active power generated by the CHP system, the microturbine and the BESS.

As you can see, the proposed methodology has efficiently managed the primary, as well as the secondary reserve, thus allowing the CHP to be distant from its limits. Furthermore, in order to recover as much as possible of the down reserve in the first hours of the day, the algorithm forced the microturbine's power output to be zero. In the other hours of the day, the algorithm coordinated the microturbine and the BESS in order to maximize as much as possible the available reserve offered by the CHP. Depending on the individual contributions to the objective function, each source of the secondary reserve was "*called*" to furnish a different amount of the active power. However, the active power of the BESS was conditioned by the cost function related to the energy stored or delivered by the BESS system over time aimed at minimizing deviations from the desired SOC.

5.2. Case 2 – Microturbine failure

This test was aimed at investigating the controller's ability to react suddenly to some troublesome events. For this purpose, starting from the previous condition, an unplanned microturbine trip was simulated at the time t = 20:00. Fig. 9 shows the time domain behavior of the active power generated by the CHP, the microturbine and the BESS. As a consequence of the microturbine fault, the isochronous controller of the master unit reacted suddenly taking complete control of the burden previously assigned to the microturbine. Then, the BESS was called up by the on-line controller to discharge the stored energy in order to restore as much as possible the primary reserve of the CHP.

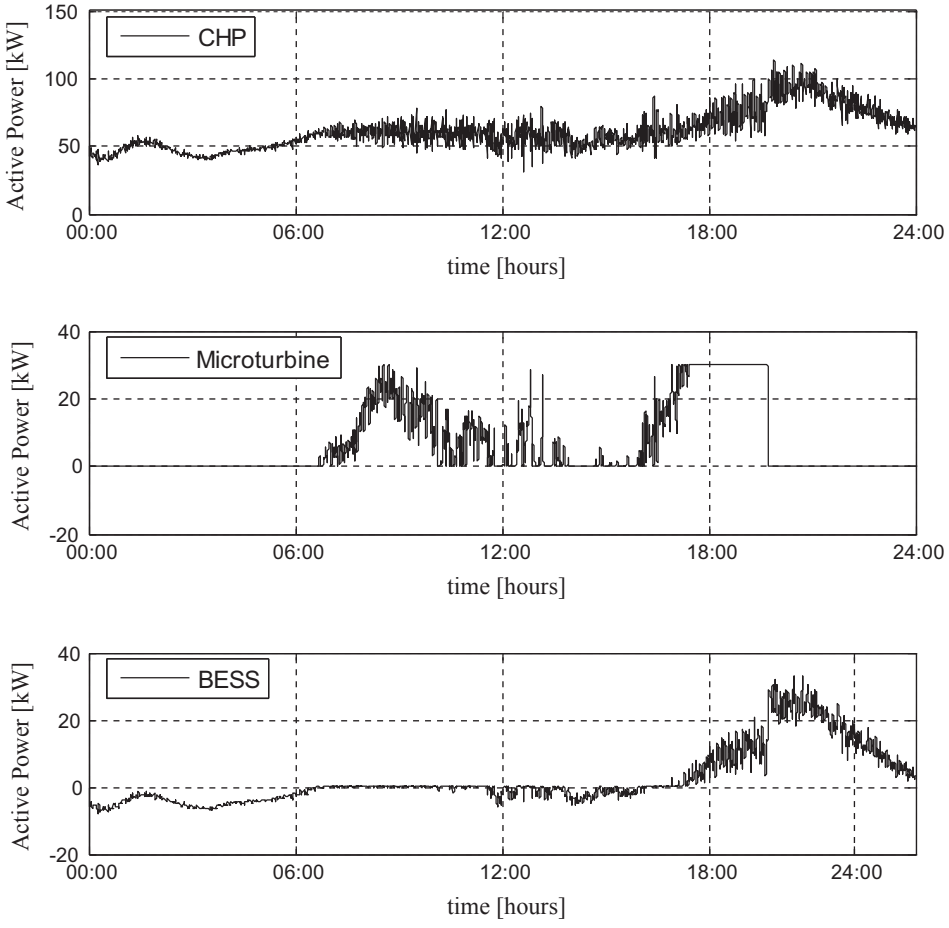

Fig. 9. Time domain behavior of the active power generated by the CHP, the microturbine and the BESS under the proposed controller.

The same conditions were used on the experimental microgrid managed on the basis of the economic dispatch. In Fig. 10, the time domain behaviors of the CHP and the microturbine are shown. As can be noted, following the microturbine tripping, the isochronous controller promptly forced the CHP to increase its active power production in order to recover the unbalance occurred to the system. At time t = 21:00, the system experienced a general blackout given by the intervention of the overcurrent relay (ANSI 50) due to trip settings which were set to be equal to 110% of the maximum active power of the CHP.

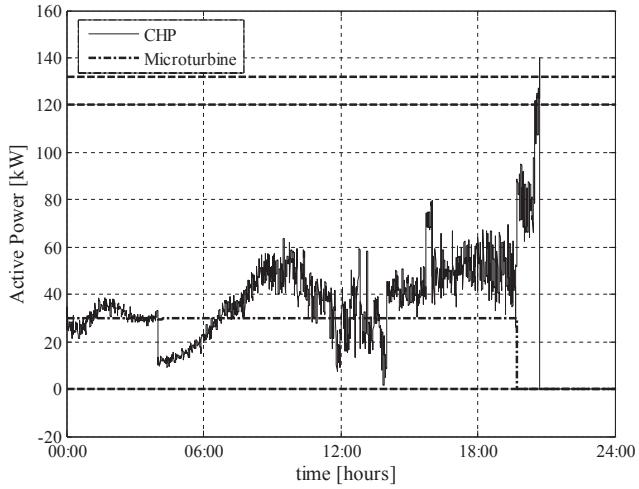

Fig. 10. Time domain behavior of the active power generated by the CHP and the Microturbine.

The greater degree of reliability achieved with the proposed controller is mainly given by its ability to automatically share the control burden of the CHP among all the remaining generators. By doing this, the proposed controller is able to guarantee more adequate reserve margins without requiring corrective control actions.

5.3. Case 3 – Annual analysis

The performances of the proposed methodology were tested on a longer time frame than the single day. With this purpose, data collected from 1st January–31st December 2016 were processed in computer simulations adopting a detailed mathematical model of the experimental microgrid. Specifically, the two following conditions were tested:

- Scenario 1 – Base Case
- Scenario 2 – N − 1 contingency analysis

Scenario 1 –Base Case.

Results obtained with the proposed controller were compared to those achieved with the economic dispatch method. For this purpose, we adopted indices based on the Expected Energy Not Supplied (ENS), on the Expected Energy for Loss of Generation to be shed (EELG), on the Expected Energy of Load to be Shed (EELS), and on the Expected Duration of Interruptions (EDI). Table 1 summarizes the obtained results.

Table 1
Comparison between the Economic dispatch and the proposed controller.

		Economic dispatch	Proposed controller
Total generated energy	[MWh/yr]	654.31	655.90
Total energy consumption	[MWh/yr]	653.31	653.48
Total energy produced/absorbed by the BESS	[MWh/yr]	−3.96/2.96	−8.56/6.15
Total duration of interruptions	**[h]**	**10**	**7**
Expected Energy Not Supplied (EENS) for generation shedding	[MWh/yr]	23.6	–
Expected Energy Not Supplied (EENS) for interruptions	[MWh/yr]	0.74	0.52
Expected Energy of Load to be Shed (EELS)	[MWh/yr]	0.16	–
Average hourly production cost for kWh	[€/kWh]	0.27	0.26
Expected total production costs	[€/yr]	176.670,00	170.530,00
Expected costs for loss of generation	[€/yr]	6.292,80	–
Expected total costs	**[€]**	**182.962,80**	**170.530,00**

If the microgrid is operated under the economic dispatch policy, the preventive control based on the load/generation shedding technique will shed 23.6 MWh of renewable generation, which correspond to 35% of the total energy production from renewables. Also the load will be curtailed for an amount of 0.16 MWh. Although the adoption of these preventive control actions could lead to the preservation of the established reserve margins, the reliability of the microgrid cannot be ensured. In fact, the real-time simulations revealed that the microgrid operated according to economic dispatch policies could experience about 10 h of energy interruption in a year, whereas the proposed controller is able to decrease the total expected duration of energy interruptions from 10 to 7 h/year without requiring any a-priori load/generation shedding. As a consequence, the comparison of the expected total costs, including the costs for the generation/load shedding, privileges the proposed methodology.

Scenario 2 – N − 1 contingency analysis.

An N − 1 contingency analysis was performed on the system in order to analyze the performances of both management methods under the loss of a generating unit or the storage device. For this purpose we assumed the following operational availabilities (see Table 2).

Table 2
Availability of the devices.

Device	Operational availability [%]
Microturbine	95,5
Photovoltaic plant	96,0
Wind Turbine	97,2
BESS	84,1

The main results of the analysis are reported in Table 3.

Also in the N − 1 contingency test, the adoption of the proposed controller improves economic performance with regard to the management under the economic dispatching policy.

6. Conclusions

The aim of this paper was to carry out a real-time coordinated control strategy able to ensure an adequate security level in islanded microgrids. The methodology can be applied to microgrids adopting the master-slave control architecture, where a specified generator takes the role of the isochronous generator for the overall system. The derived algorithm is able to regulate in the on-line environment active powers of microsources and energy storage systems of the isolated microgrid in accordance with their reserve margins and their technical limits. Control actions have been evaluated by solving a constrained dynamic optimization problem aimed at simultaneously maximizing the spinning reserve of the master unit and the duration of the regulation function of each energy storage system. The solution of this problem has been obtained by adopting an iterative algorithm involving a fictitious dynamic system in which the state variables are the active powers of microgrid sources and storage devices. The solution has been attained by adopting the direct Lyapunov theorem applied to the sensitivity theory, giving rise to an ever stable algorithm. Essentially, the adoption of the Lyapunov theorem ensured the convergence of the dynamic system to an equilibrium point corresponding to the minimum of the given multi-objective function.

Tests performed on the experimental microgrid demonstrated the ability of the proposed methodology to share the regulation burden among all sources providing the secondary reserve, thus, re-establishing reserve margins of the primary reserve offered by the selected master unit.

To sum up, the proposed methodology exhibited better results in terms of technical and economic performance compared to those obtained with the economic dispatching policy. However, test results demonstrate that some blackouts can still occur for systems with a high penetration level of nonprogrammable renewable sources. Therefore,

Table 3
Comparison between the Economic dispatch and the proposed controller.

Contingency	MT		PV		Wind Turbine		BESS	
	Economic Dispatch	On-line Controller	Economic Dispatch	On-line Controller	Economic Dispatch	On-line Controller	Economic Dispatch	On-line Controller
Duration of interruptions[a]	3	6	0	0	0	0	2	0
EENS for Gen Shed [MWh/yr]	3.19		10.27		925.94		23.36	
EELS for Load Shed [MWh/yr]	6.10		0.14		0.18		0.21	
Expected average production hourly cost for kWh [€/kWh]	0.27	0.26	0.28	0.27	0.27	0.27	0.26	0.26
Expected total production costs [€/yr]	173.970,30	172.090,20	183.080,10	180.490,80	179.470,10	178.900,60	171.130,00	172.880,00
Expected cost for generation shedding [€/yr]	857.40	–	2.876,60	–	253.90	–	6.112,60	–
Expected Total Costs [€/yr]	**174.827,70**	**172.090,20**	**185.956,70**	**180.490,80**	**179.724,00**	**178.900,60**	**177.243,10**	**172.880,00**

[a] The duration of the interruptions have been weighted with the unavailability of the device.

further developments of the methodology would require the integration in the developed controller of a preventive/corrective controller in order to increase even more the system security.

References

[1] Barklund E, Pogaku N, Prodanovic M, Hernandez-Aramburo C, Green TC. Energy management in autonomous microgrid using stability-constrained droop control of inverters. IEEE Trans Power Electron 2008;23(5):2346–52.

[2] Nutkani IU, Loh PC, Wang P, Blaabjerg F. Linear decentralized power sharing schemes for economic operation of AC microgrids. IEEE Trans Ind Electron 2016;63(1):225–34.

[3] Zhao B, Xue M, Zhang X, Wang C, Zhao J. An MAS based energy management system for a stand-alone microgrid at high altitude. Appl Energy 2015;143(April):251–61.

[4] Fang X, Yang Q, Wang J, Yan W. Coordinated dispatch in multiple cooperative autonomous islanded microgrids. Appl Energy 2016;162(January):40–8.

[5] Zhang J, Wu Y, Guo Y, Wang B, Wang H, Liu H. A hybrid harmony search algorithm with differential evolution for day-ahead scheduling problem of a microgrid with consideration of power flow constraints. Appl Energy 2016;183(December):791–804.

[6] Liu Z, Chen Y, Zhuo R, Jia H. Energy storage capacity optimization for autonomy microgrid considering CHP and EV scheduling. Appl Energy 2018;210(January):1113–25.

[7] Hirase Y, Abe K, Sugimoto K, Sakimoto K, Bevrani H, Ise T. A novel control approach for virtual synchronous generators to suppress frequency and voltage fluctuations in microgrids. Appl Energy 2018;210(January):699–710.

[8] Li J, Xiong R, Yang Q, Liang F, Zhang M, Yuan W. Design/test of a hybrid energy storage system for primary frequency control using a dynamic droop method in an isolated microgrid power system. Appl Energy 2017;201(September):257–69.

[9] Rezaei N, Kalantar M. Economic–environmental hierarchical frequency management of a droop-controlled islanded microgrid. Energy Convers Manage 2014;88(December):498–515.

[10] Rezaei N, Kalantar M. Smart microgrid hierarchical frequency control ancillary service provision based on virtual inertia concept: An integrated demand response and droop controlled distributed generation framework. Energy Convers Manage 2015;92(March):287–301.

[11] Silvente J, Kopanos GM, Pistikopoulos EN, Espuña A. A rolling horizon optimization framework for the simultaneous energy supply and demand planning in microgrids. Appl Energy 2015;155(October):485–501.

[12] Mazzola S, Astolfi M, Macchi E. A detailed model for the optimal management of a multigood microgrid. Appl Energy 2015;154(September):862–73.

[13] Nemati M, Braun M, Tenbohlen S. Optimization of unit commitment and economic dispatch in microgrids based on genetic algorithm and mixed integer linear programming. Appl Energy 2018;210(January):944–63.

[14] Marzband M, Ghadimi M, Sumper A, Domínguez-García JL. Experimental validation of a real-time energy management system using multi-period gravitational search algorithm for microgrids in islanded mode. Applied energy 2014;128(September):164–74.

[15] Lidula NWA, Rajapakse AD. Microgrids research: A review of experimental microgrids and test systems. Renew Sustain Energy Rev 2011;15(1):186–202.

[16] Eto J, Lasseter R, Schenkman B, Stevens J, Klapp D, Volkommer H, et al. Overview of the CERTS microgrid laboratory test bed. In: Integration of wide-scale renewable resources into the power delivery system, 2009 CIGRE/IEEE PES joint symposium. IEEE; July 2009. p. 1–7.

[17] Lasseter RH, Eto JH, Schenkman B, Stevens J, Vollkommer H, Klapp D, et al. CERTS microgrid laboratory test bed. IEEE Trans Power Delivery 2011;26(1):325–32.

[18] Ariyasinghe MNS, Hemapala KTMU. Microgrid test-beds and its control strategies. Smart Grid Renew Energy 2013;4(01):11–7.

[19] Moneta D, Marciandi M, Tornelli C, Mora P. Voltage optimization of a LV microgrid with DERs: field test. In: 20th International conference and exhibition on electricity distribution - Part 1, 2009, IET. June 2009. CIRED; 2009. p. 1–4.

[20] Katiraei F, Abbey C, Tang S, Gauthier M. Planned islanding on rural feeders—utility perspective. In: Power and energy society general meeting-conversion and delivery of electrical energy in the 21st century, 2008. IEEE; July 2008. p. 1–6.

[21] Loix T, Leuven KU. The first micro grid in the Netherlands: Bronsbergen. Available online on February 2009. < http://www.leonardo-energy.org/sites/leonardo-energy/files/root/pdf/2009/article2.pdf > .

[22] Loix T, Leuven KU. The residential micro grid of Am Steinweg in Stutensee, Germany. Available online on February 2009 < http://www.leonardo-energy.org/sites/leonardo-energy/files/root/pdf/2009/article3.pdf > .

[23] Barnes M, Dimeas A, Engler A, Fitzer C, Hatziargyriou N, Jones C, et al. Microgrid laboratory facilities. In: 2005 International conference on future power systems. IEEE; November 2005. p. 1–6.

[24] Cagnano A, De Tuglie E, Dicorato M, Forte G, Trovato M. PrInCE Lab experimental microgrid Planning and operation issues. In: 2015 IEEE 15th international conference on environment and electrical engineering (EEEIC). IEEE; June 2015. p. 1671–6.

[25] Cagnano A, De Tuglie E, Cicognani L. Prince—electrical energy systems lab: a pilot project for smart microgrids. Electr Power Syst Res 2017;148(July):10–7.

[26] Alharbi W, Raahemifar K. Probabilistic coordination of microgrid energy resources operation considering uncertainties. Electr Power Syst Res 2015;128(November):1–10.

[27] Lee SY, Jin YG, Yoon YT. Determining the optimal reserve capacity in a microgrid with islanded operation. IEEE Trans Power Syst 2016;31(2):1369–76.

[28] Ortega-Vazquez MA, Kirschen DS. Should the spinning reserve procurement in systems with wind power generation be deterministic or probabilistic? In: 2009 International conference on sustainable power generation and supply. IEEE; April 2009. p. 1–9.

[29] Mohan V, Singh JG, Ongsakul W. An efficient two stage stochastic optimal energy and reserve management in a microgrid. Appl Energy 2015;160(December):28–38.

[30] Alabedin AZ, El-Saadany EF, Salama MMA. Generation scheduling in microgrids under uncertainties in power generation. In: Electrical power and energy conference (EPEC), 2012 IEEE. IEEE; October 2012. p. 133–8.

[31] Zamani AG, Zakariazadeh A, Jadid S. Day-ahead resource scheduling of a renewable energy based virtual power plant. Appl Energy 2016;169(May):324–40.

[32] Wang Z, Chen B, Wang J. Decentralized energy management system for networked microgrids in grid-connected and islanded modes. IEEE Trans Smart Grid 2016;7(2):1097–105.

[33] Wang MQ, Gooi HB. Spinning reserve estimation in microgrids. IEEE Trans Power Syst 2011;26(3):1164–74.

[34] Mortezaei A, Simões MG, Al Durra A, Marafão FP, Busarello TDC. Coordinated operation in a multi-inverter based microgrid for both grid-connected and islanded modes using conservative power theory. In: Energy conversion congress and exposition (ECCE), 2015 IEEE; September 2015. p. 4602–9.

[35] Mortezaei A, Simoes MG, Marafão FP. Cooperative operation based master-slave in islanded microgrid with CPT current decomposition. In: Power & energy society general meeting, 2015 IEEE; July 2015. p. 1–5.

[36] Mortezaei A, Simoes MG, Savaghebi M, Guerrero J, Al-Durra A. Cooperative control of multi-master-slave islanded microgrid with power quality enhancement based on conservative power theory. In: IEEE transactions on smart grid. Issue 99; November 2016.

[37] Caldognetto T, Tenti P. Microgrids operation based on master–slave cooperative control. IEEE J Emerging Sel Top Power Electron 2014;2(4):1081–8.

[38] Kim JY, Jeon JH, Kim SK, Cho C, Park JH, Kim HM, et al. Cooperative control strategy of energy storage system and microsources for stabilizing the microgrid during islanded operation. IEEE Trans Power Electron 2010;25(12):3037–48.

[39] Mahmoud MS, Al-Buraiki O. Two-level control for improving the performance of MicroGrid in islanded mode. In: 2014 IEEE 23rd International symposium on industrial electronics (ISIE). IEEE; June 2014. p. 254–9.

[40] Izadbakhsh M, Gandomkar M, Rezvani A, Ahmadi A. Short-term resource scheduling of a renewable energy based microgrid. Renew Energy 2015;75(March):598–606.

[41] Mortezaei A, Simões MG, Marafão FP. Cooperative operation based master-slave in islanded microgrid with CPT current decomposition. In: 2015 IEEE power & energy society general meeting. IEEE; July 2015. p. 1–5.

[42] Vandoorn TL, Guerrero JM, De Kooning JDM, Vásquez J, Vandevelde L. Decentralized and centralized control of islanded microgrids including reserve management. In: IEEE industrial electronics magazine; 2013. p. 1–14.

[43] Rouholamini M, Rashidinejad M, Abdollahi A, Ghasemnejad H. Frequency reserve within unit commitment considering spinning reserve uncertainty. Int J Energy Eng 2012;2(4):177–83.

[44] Hernandez-Aramburo CA, Green TC, Mugniot N. Fuel consumption minimization of a microgrid. IEEE Trans Ind Appl 2005;41(3):673–81.

[45] Alharbi W, Bhattacharya K. Demand response and energy storage in MV islanded microgrids for high penetration of renewables. In: Electrical power & energy conference (EPEC), 2013 IEEE; August 2013. p. 1–6.

[46] Alabedin AZ, El-Saadany EF, Salama MMA. Generation scheduling in microgrids under uncertainties in power generation. In: Electrical power and energy conference (EPEC), 2012 IEEE; October 2012. p. 133–8.

Alessia Cagnano received B.Sc. and M.Sc. degree in Electrical Engineering from the Polytechnic of Bari (Italy) in 2005 and 2007 respectively. She received the Ph.D. degree in Electrical Engineering at the Polytechnic of Bari in 2011. Her research interests include microgrid control and operation, and power system analysis and control.

Angelo Caldarulo Bugliari received B.Sc. and M.Sc. degree in Electrical Engineering, in 2012 and 2016 respectively, from the Polytechnic University of Bari (Italy), where he is currently cooperating with Electrical Energy Systems research group. His research interest concerns microgrids operation and control and power systems economics, analysis and planning.

Enrico De Tuglie received the M.Sc. and Ph.D. degrees in electrical engineering from the Polytechnic of Bari. He has been visiting scientist at the Pacific Northwest National Laboratory (PNNL) operated by Battelle under the Department Of Energy (USA). Since December 2003 he has been Associate Professor at the Polytechnic of Bari. His research interests include power system analysis and control and reregulated markets.